Electronic Supplementary Material (ESI) for Journal of Materials Chemistry C.

Supporting Information for

Optical temperature sensing properties and thermoluminescence behavior in Er-modified potassium sodium niobate-based multifunctional ferroelectric ceramics

Wei Li[1], Di Wang[1], Xuefeng Li[2], Peng Li[1], Peng Fu[1], Chengchao Hu[1], Jigong Hao[1,*], Wei Li[1,*], Qiwei Zhang[2,*]

[1]*School of Materials Science and Engineering, Liaocheng University, Liaocheng 252059, China.*

[2]*Inner Mongolia Key Laboratory of Ferroelectric-related New Energy Materials and Devices, School of Materials and Metallurgy, Inner Mongolia University of Science and Technology, Baotou 014010, China.*

[*]Corresponding authors. E-mail addresses: haojigong@lcu.edu.cn (J. Hao); liwei_727@163.com (W. Li); zqw8000@imust.edu.cn (Q. Zhang)

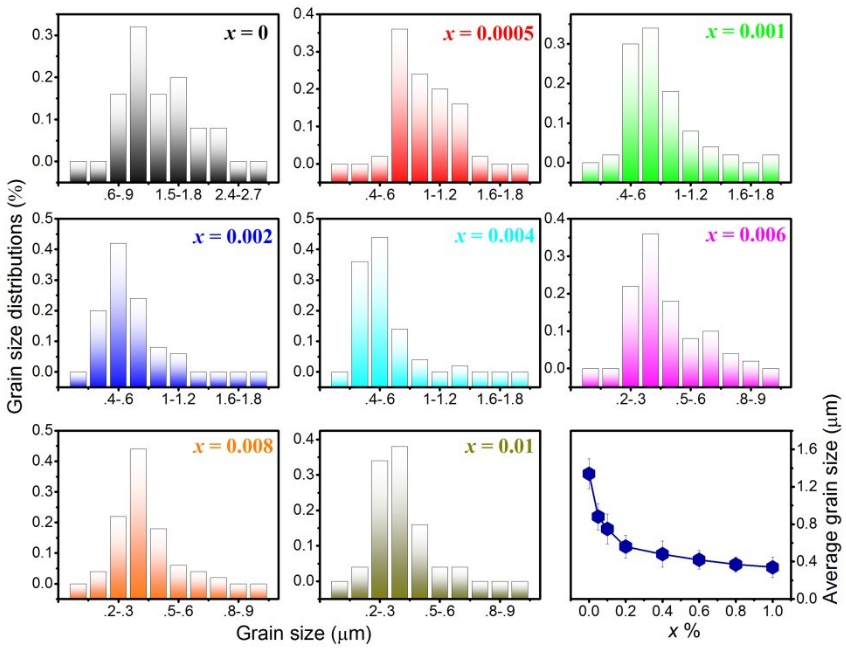

Fig. S1. The grain size distribution and the average grain size of *x*Er ceramics.

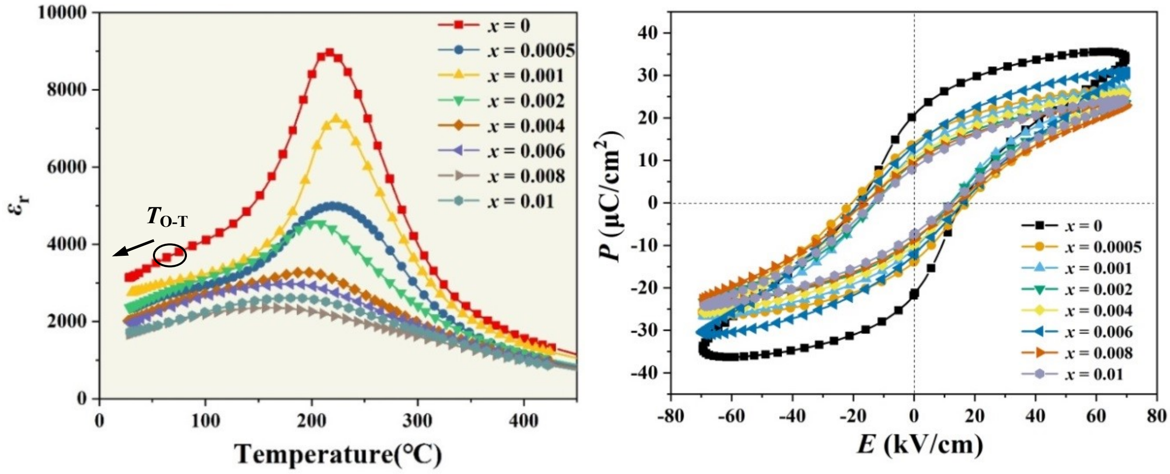

Fig. S2. (a) The dielectric constant (ε_r) as a function of temperature for the *x*Er ceramics recorded at 100 kHz. (b) The polarization-electric field hysteresis loop for the *x*Er ceramics recorded at room temperature and 10 Hz.

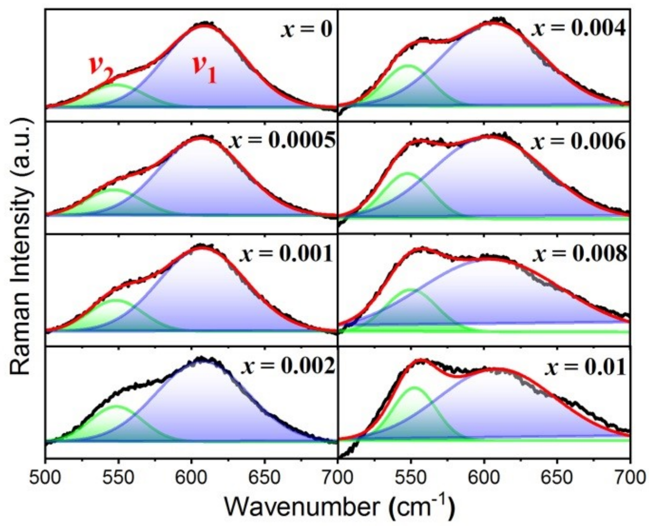

Fig. S3. The fitting results of Lorentz function of Raman peaks based on E_g (v_2) and A_{1g} (v_1) modes, for *x*Er ceramics.

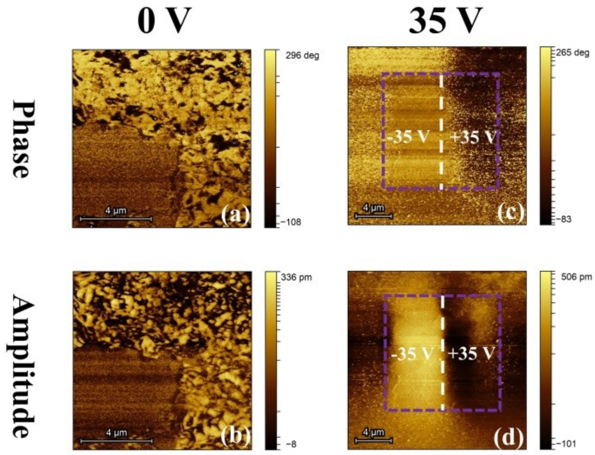

Fig. S4. The PFM images for amplitude and phase of the *x*Er ceramics with $x = 0$ without poling and after poling with the dc voltage of ±35V.

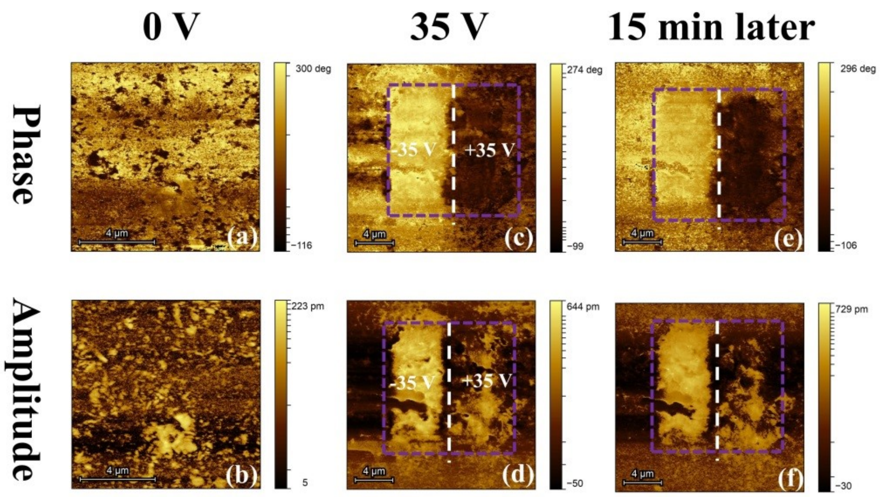

Fig. S5. The PFM images for amplitude and phase of the *x*Er ceramics with $x = 0.004$ without poling and after poling with the dc voltage of ±35V.

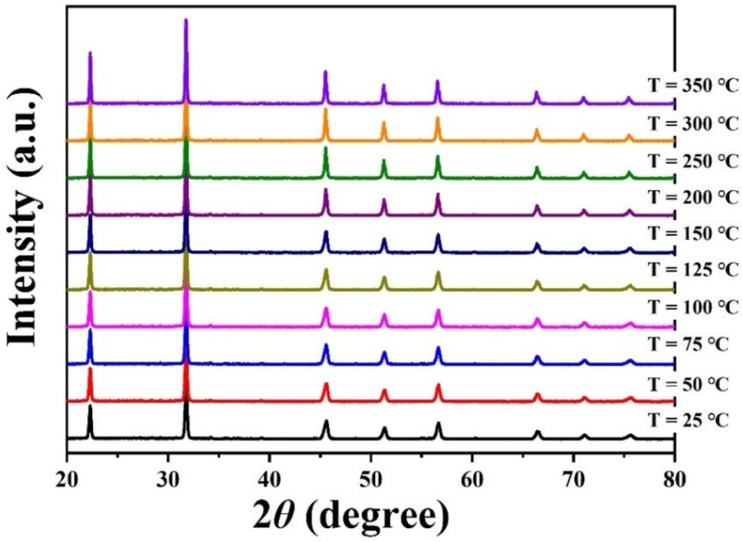

Fig. S6. The XRD patterns of 0.0005Er ceramic at different temperatures.

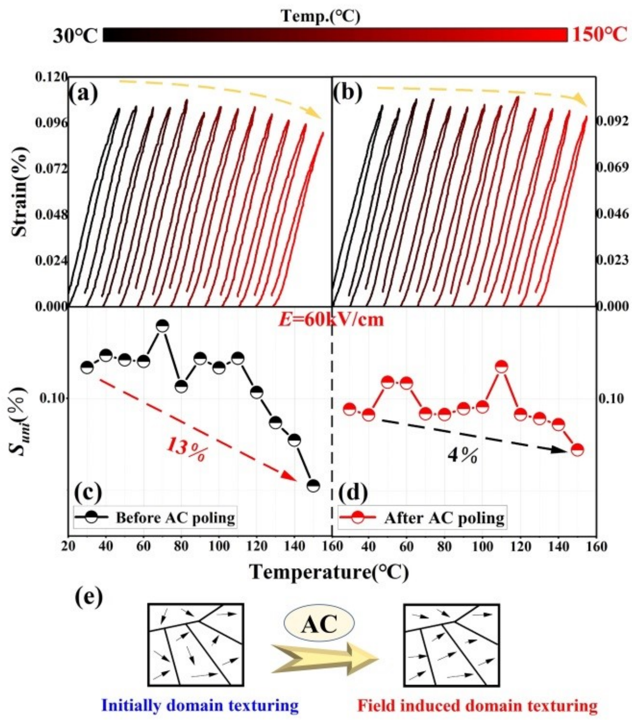

Fig. S7. (a,b) Unipolar strain curves of xEr (x = 0.001) sample at different temperatures before and after poling, (c,d) Change of S_{uni} values with temperature for samples before and after poling. (e) The state of the domain and after poling.

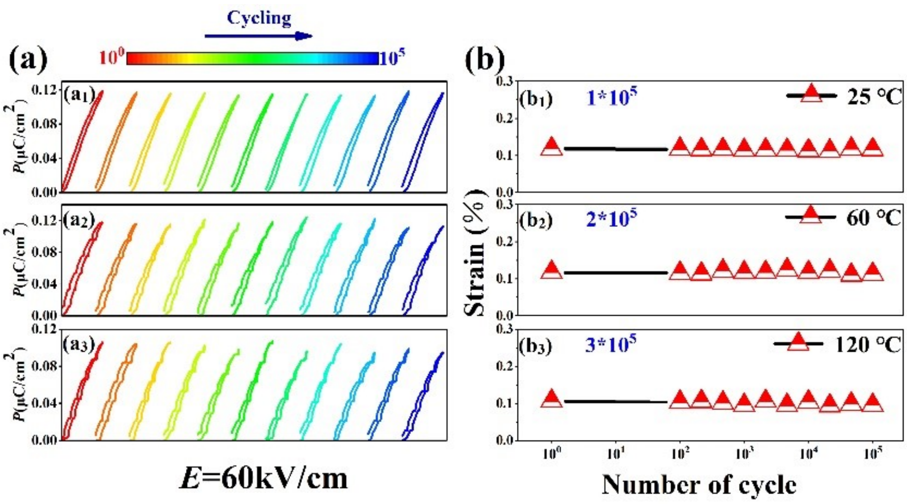

Fig. S8. The evolution of (a) unipolar *S*–*E* curves and (b) unipolar S_{uni} values with electric field cycling at different temperatures, for *x*Er (x = 0.0005) sample.

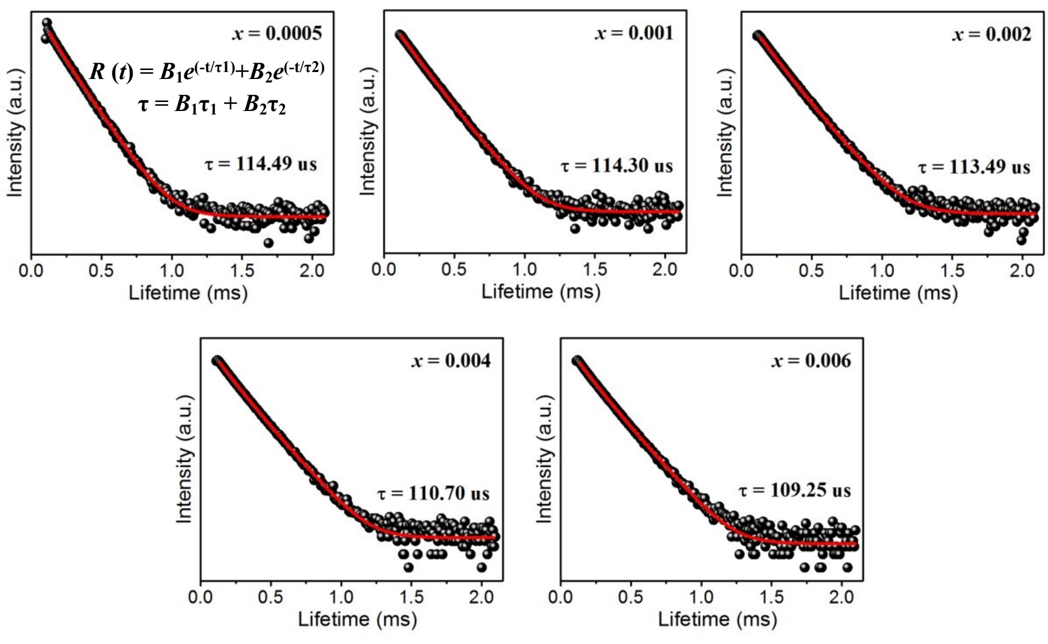

Fig. S9. The PL decay curves of the *x*Er samples.

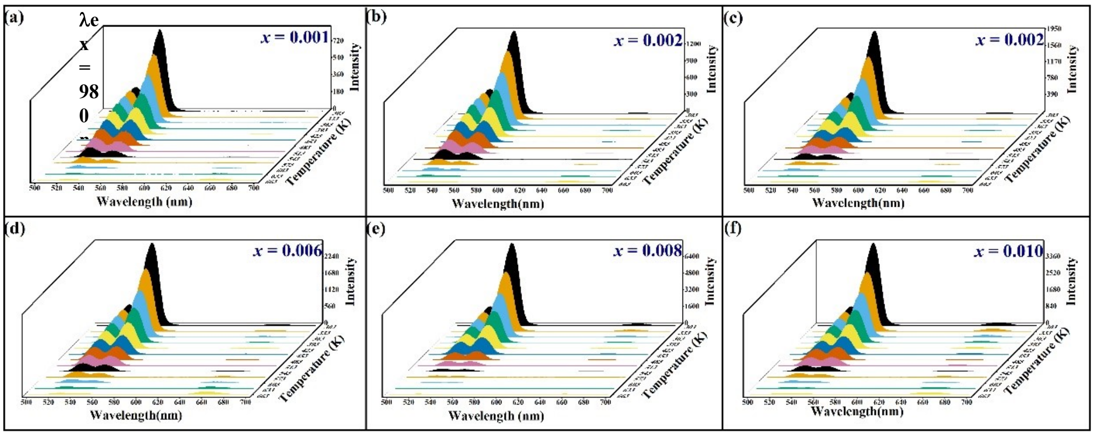

Fig. S10. UC emission spectra of *x*Er ceramics measured in the temperature range of 303–663 K.

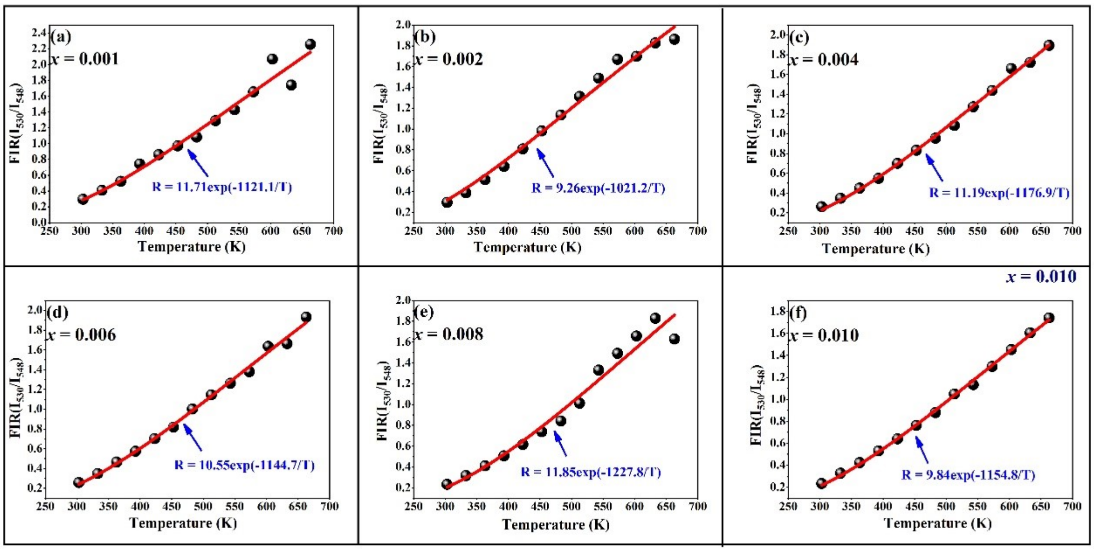

Fig. S11. Temperature dependent FIR for *x*Er ceramics

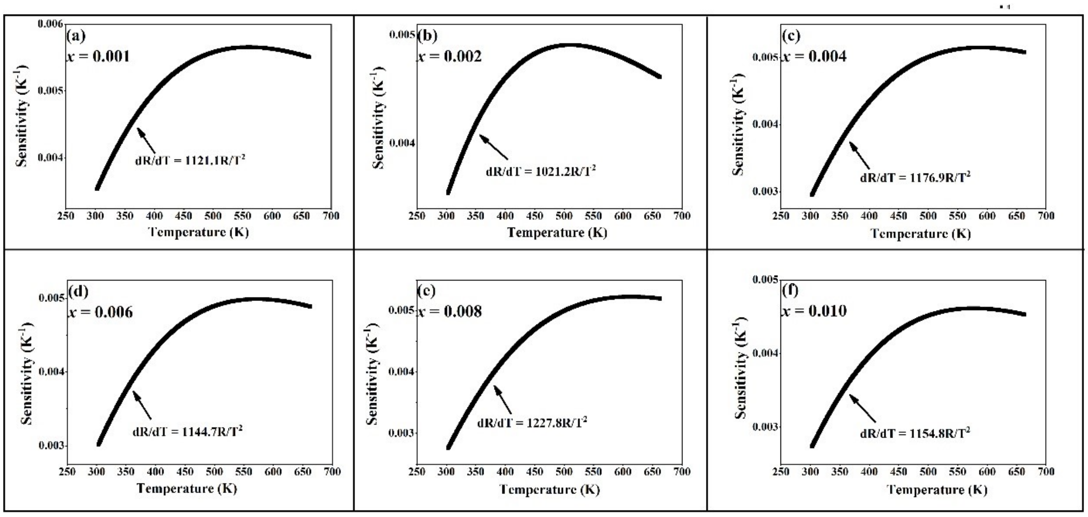

Fig. S12. The sensor sensitivity as a function of temperature for *x*Er ceramics

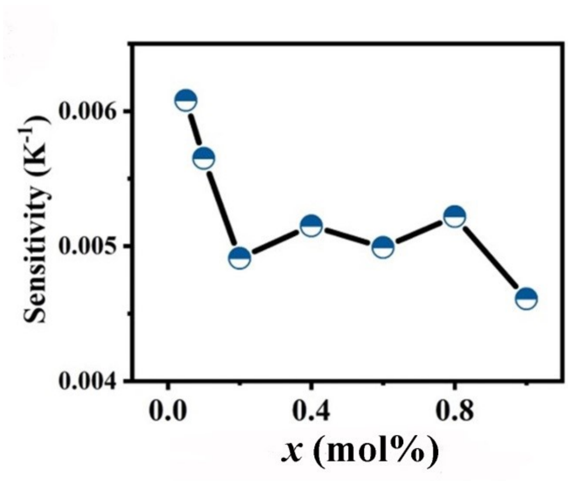

Fig. S13. Change of the maximum sensitivity values with compositions, for *x*Er ceramics.

Table S1 Rietveld refinement parameters of *x*Er ceramics.

Sample	R_{wp} (%)	R_p (%)	λ^2	Space group	Phase	Phase frac. (%)	a (Å)	b (Å)	c (Å)
x=0	4.70	3.63	2.050	*Amm2*	Orthorhombic	33%	3.99218	5.61034	5.72411
				P4mm	Tetragonal	67%	3.97510	3.97510	3.99934
x=0.0005	5.04	3.47	2.332	*Amm2*	Orthorhombic	19%	3.93122	5.65390	5.64606
				P4mm	Tetragonal	81%	3.97470	3.97470	3.99471
x=0.001	4.80	3.54	1.606	*P4mm*	Tetragonal	100%	3.97228	3.97228	3.99577
x=0.002	5.45	4.07	2.567	*P4mm*	Tetragonal	100%	3.98185	3.98185	3.97303
x=0.004	5.29	4.13	2.278	*P4mm*	Tetragonal	100%	3.98261	3.98261	3.96816
x=0.006	4.33	3.40	1.650	*P4mm*	Tetragonal	100%	3.97080	3.97080	3.98135
x=0.008	4.39	3.49	1.902	*P4mm*	Tetragonal	100%	3.97085	3.97085	3.99083
x=0.010	4.74	3.69	2.181	*P4mm*	Tetragonal	100%	3.96325	3.96325	3.98637

Table S2 Rietveld refinement parameters of the x = 0.0005 sample at different temperatures.

T (°C)	R_{wp} (%)	R_p (%)	λ^2	Space group	Phase	Phase frac. (%)	a (Å)	b (Å)	c (Å)
25	7.42	5.46	3.345	*Amm2*	Orthorhombic	19	3.96628	5.62653	5.61901
				P4mm	Tetragonal	81	3.97115	3.97115	3.99206
75	7.49	5.61	3.358	*Amm2*	Orthorhombic	9	3.96865	5.62561	5.62571
				P4mm	Tetragonal	91	3.97208	3.97208	3.99461
100	7.89	5.94	2.949	*P4mm*	Tetragonal	100	3.97243	3.97243	3.99072

Table. S3. The comparison of optical temperature sensing performance of different Er-doped materials without Yb co-doping.

RE ions: host	Temperature range (K)	Maximum sensitivity (K^{-1})	Excitation wavelength (nm)	Refs
Er: KNNS-0.04BNKZ	303-663	0.0061	980	This work
Er: BCPT	100-560	0.0035	980	[44]
Er: BNT-BT-SBT	300-600	0.0055	980	[45]
Er: BCT	103-573	0.0033	980	[46]
Er: BT-0.07NT	120-560	0.00042	980	[47]
Er: KNLN-NT	83-583	0.0045	980	[48]
Er: KNN-0.4LN	83-503	0.0026	980	[49]
Er: BCT-BZT	200-443	0.0044	980	[16]
Er: NBT nanocrystal	80-480	0.0053	980	[50]
Er: $Na_{0.5}Er_{0.5}Bi_4Ti_4O_{15}$	173-503	0.0017	980	[51]
Er: NBN	293-753	0.00524	980	[52]
Er: fluorotellurite glass	293-540	0.0054	800	[53]
Er: BTW	83-423	0.0031	980	[54]
Er-Mo: $Yb_3Al_5O_3$	295-973	0.0048	976	[55]
Er: $Na_{0.82}Ca_{0.08}Er_{0.16}Y_{0.853}F_4$	5-300	0.0022	980	[56]
Er: KYb_2F_7 nano-crystals glass ceramic	300-480	0.0043	980	[57]

Table. S4. The comparison of optical temperature sensing performance of different Er-doped ferroelectric materials.

RE ions: host	Temperature range (K)	Maximum sensitivity (K^{-1})	Excitation wavelength (nm)	Refs
Er: KNNS-0.04BNKZ	303-663	0.0061	980	This work
Er/Yb: KNN-0.4LN	83-663	0.0060	980	[49]
Er: KNN-0.4LN	83-503	0.0026	980	[49]
Er: KNLN-NT	83-583	0.0045	980	[48]
Er: NBN	293-713	0.00524	980	[52]
Er: NBT nanocrystal	80-480	0.0053	980	[50]
Er/Yb: NBT	175-553	0.0035	980	[58]
Er: BT-0.07NT	120-560	0.0042	980	[47]
Er/Yb: BT nanocrystal	120-505	0.0048	980	[59]
Er/Yb: BCT-BZT	173-573	0.0068	980	[60]
Er: BCPT	100-560	0.0035	980	[44]
Er: BCT-BZT	200-443	0.0044	980	[16]
Er: BNT-BT-SBT	300-600	0.0055	980	[45]
Er/Yb: PLZT	140-320	0.0022	980	[61]
Er: PIN-PMN-PT	160-360	0.0035	980	[62]